

Article

# BCS Class IV Oral Drugs and Absorption Windows: Regional-Dependent Intestinal Permeability of Furosemide

Milica Markovic <sup>1</sup>, Moran Zur <sup>1</sup>, Inna Ragatsky <sup>1</sup>, Sandra Cvijic <sup>2</sup> and Arik Dahan <sup>1,\*</sup>

<sup>1</sup> Department of Clinical Pharmacology, School of Pharmacy, Faculty of Health Sciences, Ben-Gurion University of the Negev, Beer-Sheva 8410501, Israel; milica@post.bgu.ac.il (M.M.); moranfa@post.bgu.ac.il (M.Z.); inna.ragatsky@gmail.com (I.R.)

<sup>2</sup> Department of Pharmaceutical Technology and Cosmetology, Faculty of Pharmacy, University of Belgrade, Vojvode Stepe 450, 11221 Belgrade, Serbia; sandra.cvijic@pharmacy.bg.ac.rs

\* Correspondence: arikd@bgu.ac.il; Tel.: +972-8-647-9483; Fax: +972-8-647-9303

Received: 16 November 2020; Accepted: 30 November 2020; Published: 2 December 2020



**Abstract:** Biopharmaceutical classification system (BCS) class IV drugs (low-solubility low-permeability) are generally poor drug candidates, yet, ~5% of oral drugs on the market belong to this class. While solubility is often predictable, intestinal permeability is rather complicated and highly dependent on many biochemical/physiological parameters. In this work, we investigated the solubility/permeability of BCS class IV drug, furosemide, considering the complexity of the entire small intestine (SI). Furosemide solubility, physicochemical properties, and intestinal permeability were thoroughly investigated in-vitro and in-vivo throughout the SI. In addition, advanced in-silico simulations (GastroPlus<sup>®</sup>) were used to elucidate furosemide regional-dependent absorption pattern. Metoprolol was used as the low/high permeability class boundary. Furosemide was found to be a low-solubility compound. Log D of furosemide at the three pH values 6.5, 7.0, and 7.5 (representing the conditions throughout the SI) showed a downward trend. Similarly, segmental-dependent in-vivo intestinal permeability was revealed; as the intestinal region becomes progressively distal, and the pH gradually increases, the permeability of furosemide significantly decreased. The opposite trend was evident for metoprolol. Theoretical physicochemical analysis based on ionization,  $pK_a$ , and partitioning predicted the same trend and confirmed the experimental results. Computational simulations clearly showed the effect of furosemide's regional-dependent permeability on its absorption, as well as the critical role of the drug's absorption window on the overall bioavailability. The data reveals the absorption window of furosemide in the proximal SI, allowing adequate absorption and consequent effect, despite its class IV characteristics. Nevertheless, this absorption window so early on in the SI rules out the suitability of controlled-release furosemide formulations, as confirmed by the in-silico results. The potential link between segmental-dependent intestinal permeability and adequate oral absorption of BCS Class IV drugs may aid to develop challenging drugs as successful oral products.

**Keywords:** BCS class IV drugs; segmental-dependent intestinal permeability; intestinal absorption; oral drug delivery; biopharmaceutics; physiologically-based pharmacokinetic (PBPK) modeling; furosemide

## 1. Introduction

The biopharmaceutical classification system (BCS) developed by Amidon et al. revealed that the solubility/dissolution of the drug and its intestinal permeability are the two key factors that dictate drug absorption following oral administration [1,2]. Drug solubility in the gastrointestinal milieu may change in different intestinal segments, e.g., due to pH changes, in a fairly predictable

manner; depending on the pKa, the solubility of acidic drugs may increase as the luminal pH rises in more distal regions of the small intestine, and vice versa for basic drugs [3–5]. On the other hand, time- and segmental-dependent intestinal permeability is more complicated and harder to predict [1]. Mechanisms contributing to segmental-dependent permeability throughout the gastrointestinal tract (GIT) include different morphology along the GIT, variable intestinal mucosal cell differentiation, changes in the drug concentration (in case of carrier-mediated transport), modulation of tight junction permeability, and luminal contents and properties, e.g., pH, transporter expression, variability in the structure/composition of the intestinal membrane itself, and more [6–11].

The four BCS classes highlight the limiting factors of the absorption process: (1) Class I, high-solubility high-permeability drugs, indicate the easier and straightforward development process, and complete absorption is expected; (2) Class II, low-solubility high-permeability drugs, indicate that a solubility/dissolution limitation is expected; (3) Class III, high-solubility low-permeability drugs, indicate that the intestinal absorption of this class of drugs will be limited by the permeability rate; and (4) Class IV, low-solubility low-permeability drugs [12]. Since Class IV drugs suffer from inadequate solubility and permeability, they have very poor oral bioavailability and are inclined to exhibit very large inter- and in-subject variability. Therefore, unless the drug dose is very low, they are generally poor oral drug candidates. Yet, according to some estimates, ~5% of the world's top oral drugs belong to this class [13–15]. In some cases, this is due to the absorption window, which is often critical for the success or failure of a certain drug. In order to gather information about the drug absorption window, extensive work and thorough analysis of luminal conditions and drug absorption is needed, within different locations throughout the GIT. Here, we present such analysis for BCS class IV drug, furosemide [16].

Furosemide is a powerful loop diuretic and is indicated for treating edematous conditions associated with heart, renal, and hepatic failure, as well as for the treatment of hypertension [17,18]. Drug therapy with furosemide is often complex, due to apparent erratic oral systemic availability and unpredictable responses to an administered dose [19]. Even though furosemide is a class IV drug, it is a very common and widely prescribed drug on the market.

In this work, we aimed to investigate the reason for apparent success of furosemide as a marketed product, despite its poor biopharmaceutical properties, and classification as BCS class IV drug, in order to allow development of future class IV compounds. We posit that segmental-dependent permeability of furosemide may contribute to its absorption complexity and provide a certain absorption window in which the drug has suitable permeability and, hence, gets absorbed. For this reason, we investigated the in-vivo intestinal permeability of furosemide throughout different segments of the small intestine. Solubility studies, as well as theoretical physicochemical analysis of furosemide and advanced modern in-silico GastroPlus® simulations, were performed, in order to elucidate the mechanistic reasons behind the experimental results. Furosemide data were compared to the  $\beta$ -blocker metoprolol, the Food and Drug Administration (FDA) reference drug for the low/high permeability class boundary. Overall, this experimental setup allowed us to reveal important insights on the performance of furosemide, despite its unfavorable drug-like properties, and discuss extrapolation of these insights to other BCS class IV drug candidates.

## 2. Methods

### 2.1. Materials

Furosemide, metoprolol, phenol red, potassium chloride, potassium phosphate monobasic, potassium phosphate dibasic, sodium chloride, acetic acid, maleic acid, *n*-octanol, and trifluoroacetic acid (TFA) were all purchased from Sigma Chemical Co. (St. Louis, MO, USA). Acetonitrile and water, ultra-performance liquid chromatography (UPLC) grade were purchased from Merck KGaA, Darmstadt, Germany. Remaining chemicals were of analytical reagent grade.

## 2.2. Solubility Studies

The pH-dependent solubility studies were performed using the shake flask method, as previously reported [20–23]. The equilibrium solubility of furosemide was determined at both 37 °C and at room temperature (25 °C), in phosphate buffer pH 7.5, acetate buffer pH 4.0, and maleate buffer pH 1.0. Surplus quantity of furosemide was introduced to glass vials holding buffer solutions with different pH; the pH of those solutions was measured following drug addition to the buffers and, consequently, placed in the shaking incubator (100 rpm) at 37 °C. The vials were centrifuged (10,000 rpm, 10 min), and the supernatant was instantly analyzed by UPLC. The dose number for furosemide was calculated using the established equation:  $D_0 = M/V_0/C_s$ ;  $M$  being the highest single-unit dose strength of furosemide (taken as 80 mg [24]),  $V_0$  is the initial volume of water (250 mL), and  $C_s$  is the solubility at each pH; the drug is considered highly soluble if the  $D_0 < 1$ .

## 2.3. Evaluation of Octanol-Buffer Partition Coefficients (Log D)

Furosemide and metoprolol experimental octanol-buffer partition coefficients (Log D) were studied at pH 6.5, 7.0, and 7.5 using the shake-flask method [8,11]. Drug solutions in octanol-saturated phosphate buffer (pH 6.5, 7.0, 7.5) were equilibrated at 37 °C for 48 h. The octanol and water phase were divided via centrifugation, and the drug content in the water phase was quantified using UPLC; the furosemide/metoprolol concentration in the octanol phase was determined by mass balance.

## 2.4. Physicochemical Analysis

The theoretical fraction extracted into octanol ( $f_e$ ) was calculated using the following equation [25,26].

$$f_e = \frac{f_u P}{1 + f_u P'}$$

in which  $P$  represents the octanol-water partition coefficient of the unionized drug form, and  $f_u$  is the fraction unionized of the drug at a certain pH. Experimental Log  $P$  values were taken from the literature for both furosemide (2.29) [27] and metoprolol (2.19) [28]. The  $f_u$  versus pH was plotted according to the Henderson-Hasselbalch equation, using the  $pK_a$  literature values: 9.68 for metoprolol [29] and 3.8 for furosemide [24].

## 2.5. Rat Single-Pass Intestinal Perfusion

Effective permeability coefficient ( $P_{eff}$ ) of furosemide versus metoprolol in various intestinal segments was assessed using the single-pass rat intestinal perfusion (SPIP) in-vivo model. The murine studies were completed according to the approved protocol by Ben-Gurion University of the Negev Animal Use and Care Committee (Protocol IL-08-01-2015). The animals (male Wistar rats weighing 230–260 g, Harlan, Israel) were housed and handled according to Ben-Gurion University of the Negev Unit for Laboratory Animal Medicine Guidelines. All animals were fasted overnight (12–18 h) with free access to water; rats were randomly allocated to different experimental groups. The intestinal perfusion study was performed according to the previous reports [7,9,30–32]. Animals were anesthetized via intramuscular injection of 1 mL/kg ketamine-xylazine solution (9%:1%) and placed on a heated (37 °C) surface (Harvard Apparatus Inc., Holliston, MA, USA); the rat abdomen was uncovered via a midline incision (~3 cm). Permeability ( $P_{eff}$ ) was measured in proximal jejunum (starting 2 cm lower from the ligament of Treitz), mid-small intestine (SI) segment (isolated between the end of the upper and the beginning of the lower segments), and distal segment of the ileum (ending 2 cm above the cecum) accounting for the complexity of the entire SI [7]. Intestinal segments were cannulated on both ends and perfused with drug-free buffer. Working solutions containing furosemide (320 µg/mL), metoprolol (400 µg/mL), and phenol red (a non-absorbable marker for water flux measurements) were prepared with potassium phosphate monobasic and sodium phosphate dibasic, to achieve pH of 6.5, 7.0 and 7.5; osmolarity (290 mOsm/L) and ionic strength in all buffers was maintained throughout the study.

Drug solutions were incubated in a 37 °C water bath. Steady-state environment was ensured by perfusing the drug-containing buffer for 1 h, followed by additional 1 h of perfusion, during which sampling was done every 10 min. The pH of the collected samples was measured in the outlet sample to verify that there was no pH change throughout the perfusion. All samples were assayed by UPLC. The length of each perfused intestinal segment was measured in the end of the experiment. The effective permeability ( $P_{\text{eff}}$ ; cm/s) through the rat SI wall was calculated according to the following equation:

$$P_{\text{eff}} = \frac{-Q \ln (C'_{\text{out}}/C'_{\text{in}})}{2\pi RL},$$

in which Q is the perfusion buffer flow rate (0.2 mL/min);  $C'_{\text{out}}/C'_{\text{in}}$  is the ratio of the outlet/inlet drug concentration adjusted for water transport; R is the radius of the intestinal segment (conventionally used as 0.2 cm); and L is the exact length of the perfused SI segment as was measured at the experiment endpoint [7,33,34].

## 2.6. Analytical Methods

Concentration of furosemide and metoprolol was evaluated using an UPLC instrument Waters Acquity UPLC H-Class (Milford, MA, USA), with a photodiode array detector and Empower software. Furosemide and metoprolol were separated on Acquity UPLC XTerra C18 3.5  $\mu\text{m}$  4.6 mm  $\times$  250 mm column (Waters Co., Milford, MA, USA). Gradient mobile phase, going from 70:30% to 90:10% *v/v* 0.1% trifluoroacetic acid in water/acetonitrile, respectively, on a flow rate of 1 mL/min (25 °C). The inter- and intraday coefficients of variation were < 1.0% and 0.5%, respectively.

## 2.7. Statistics

Solubility studies were performed in four replicates; Log D studies were performed in six replicates, whereas animal perfusion studies were  $n = 4$ . Values are expressed as means  $\pm$  standard deviation (SD). To determine statistically significant differences among the experimental groups, a 2-tailed nonparametric Mann–Whitney U test for 2-group comparison was used;  $p < 0.05$  was termed significant.

## 2.8. In-Silico Simulations

Computer simulations of furosemide absorption and concomitant plasma concentrations following oral administration in humans were conducted using GastroPlus<sup>TM</sup> software package (v. 9.7.0009, 2019, Simulations Plus Inc., Lancaster, CA, USA). The required input data regarding drug physicochemical and pharmacokinetic properties were experimentally determined, taken from literature or in-silico predicted. Human permeability values throughout the SI were calculated from the experimental rat single-pass intestinal perfusion data, using the software integrated “permeability converter”. Drug disposition was best described by three-compartmental pharmacokinetic model, whereas the relevant parameters (clearance (CL), volume of distribution (Vd) and distribution constants between central and peripheral compartments) were estimated using PKPlus software module, based on the in-vivo plasma concentration data for an intravenous (i.v.) bolus dose [35]. The application of three-compartmental model to describe furosemide pharmacokinetics has already been reported in literature [36,37]. Graphical data from literature were digitized using DigIt<sup>TM</sup> program (version 1.0.4, 2001–2008, Simulations Plus, Inc., Lancaster, CA, USA). Physiological parameters were the software default values representing fasted state physiology of a healthy human representative.

The software simulates drug absorption from the GIT using the integrated Advanced Compartment Absorption and Transit (ACAT) GIT model that consists of nine compartments (stomach, duodenum, two segments of jejunum, three segments of ileum, caecum, and ascendant colon). These compartments are linked in series, and the amount of drug dissolved and absorbed from each compartment is calculated by the system of differential equations. More details on the ACAT model can be found

in the literature [38,39]. Regarding the fact that furosemide is a poorly-soluble drug, the model accounted for the effect of bile salt on drug solubility and diffusion coefficient. Drug dissolution rate under physiological conditions was predicted using the software default Johnson dissolution equation (based on modified Nernst-Bruner equation) [40].

The validity of the model (i.e., the selection of input values) was validated by comparison of the prediction results (bioavailability (F), maximum plasma concentration ( $C_{max}$ ), time to reach  $C_{max}$  ( $t_{max}$ ), and area under the plasma concentration-time curve ( $AUC_{0-\infty}$ )) with published data from the in-vivo studies for peroral (p.o.) drug administration. Percent prediction error (%PE) between the predicted and mean in-vivo observed data from a clinical study was calculated using the following equation:

$$\%PE = \frac{(\text{Observed value} - \text{Predicted value}) \times 100}{\text{Observed value}}$$

In the next step, the generated model was used to mechanistically interpret furosemide regional absorption pattern, and to estimate the outcomes for various hypothetical drug dissolution scenarios (illustrating drug dissolution from immediate-release (IR) and controlled-release (CR) oral formulations). In the last case, hypothetical dissolution profiles were used as additional inputs to describe drug release rate in-vivo, and the selected dosage form was “CR dispersed” to allow input of the tabulated dissolution data.

### 3. Results

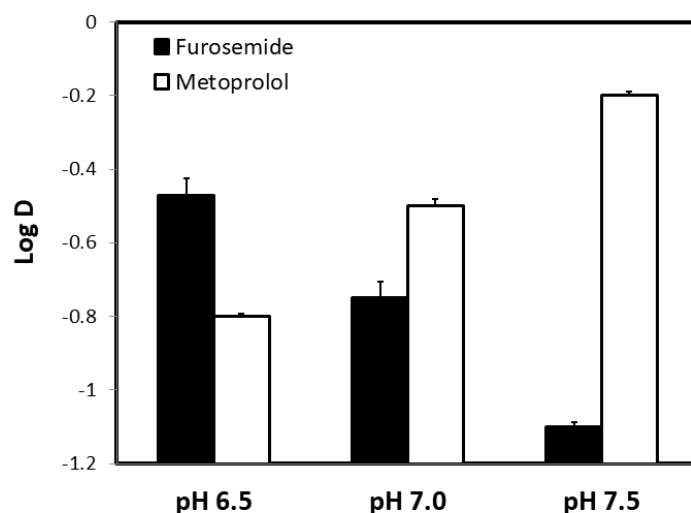
The solubility values obtained for furosemide at 37 °C and at room temperature (25 °C) are summarized in Table 1, as well as the corresponding dose number ( $D_0$ ). Furosemide showed pH-dependent solubility, in accordance with its acidic nature. It can be seen that, while, at pH 7.5, furosemide has suitable solubility (as evident by  $D_0$  lower than 1), at the lower pH values, 1.0 and 4.0, it is poorly soluble. When taking 80 mg as the highest dose strength, although  $D_0 < 1$  was obtained at pH 7.5, at pH 1.0 and 4.0, the  $D_0$  is higher than 1; hence, furosemide was found to be a low-solubility compound according to the BCS.

**Table 1.** Furosemide solubility values ( $\mu\text{g/mL}$ ) at the three pH values 1.0, 4.0, and 7.5, at 37 °C (upper panel), and at room temperature (25 °C; lower panel), as well as the corresponding dose number ( $D_0$ ) calculated for an 80-mg dose. Data presented as mean  $\pm$  SD;  $n = 6$ .

At 37 °C		
pH	Solubility ( $\mu\text{g/mL}$ )	Corresponding $D_0$
1	19.4 $\pm$ 3.7	16.5
4	65.5 $\pm$ 9.0	4.8
7.5	8340.1 $\pm$ 81.6	0.04
At 25 °C		
pH	Solubility ( $\mu\text{g/mL}$ )	Corresponding $D_0$
1	40.3 $\pm$ 16.2	7.9
4	56.7 $\pm$ 12.2	5.6
7.5	8550.6 $\pm$ 149.4	0.04

Octanol-buffer partition coefficient values of furosemide and metoprolol at the three pH values 6.5, 7.0, and 7.5 (representing the conditions throughout the small intestine) are presented in Figure 1. Both drugs presented a clear pH-dependent Log D values across the studied pH range, with opposite trends; while furosemide’s partitioning decreases as the pH rises, metoprolol shows higher partitioning into octanol at higher pH (metoprolol is the acceptable reference drug for the low/high permeability class boundary). In addition, furosemide’s Log D at pH 6.5 was higher than that of metoprolol at the same pH; this is a surprising finding since Log D may sometimes be used as a surrogate for passive

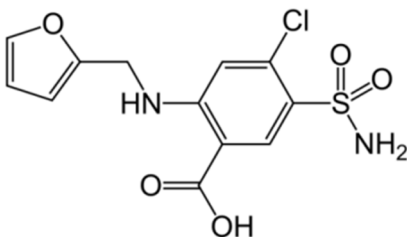
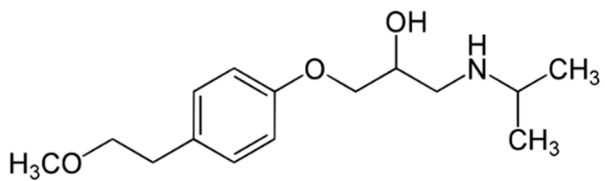
permeability. Indeed, at higher pH values (7.0 and 7.5), metoprolol Log D increases, while furosemide decreases, and metoprolol Log D becomes higher than furosemide.



**Figure 1.** The octanol-buffer partition coefficients, Log D, for furosemide and metoprolol at the three pH values 6.5, 7.0, and 7.5. Data are presented as the mean  $\pm$  S.D.;  $n = 6$  in each experimental group.

Furosemide and metoprolol physicochemical properties are presented in Table 2. Figure 2 presents furosemide versus metoprolol theoretical fraction unionized ( $f_u$ ) and fraction extracted into octanol ( $f_e$ ) as a function of pH. The plots have a standard sigmoidal shape, with opposite trends for furosemide vs. metoprolol. The  $f_e$  vs. pH plot follows the same pattern to the  $f_u$  plot, only with a shift to the right (higher pH values) for acidic drug (furosemide), and to the left (lower pH values) for basic (metoprolol) drugs. The shift magnitude in both cases equals  $\text{Log}(P - 1)$  at the midpoint of the  $f_e$  and  $f_u$  curves [25,26]. The experimental drug octanol-buffer partitioning at the three pH values (6.5, 7.0, and 7.5) are illustrated in Figure 2, as well, and it can be seen that they were in excellent agreement with the theoretical plots.

**Table 2.** Physicochemical parameters and chemical structure of furosemide and metoprolol.

Drug	Chemical Structure	pK <sub>a</sub>	Log P	PSA
Furosemide		3.8	2.3	127.7
Metoprolol		9.7	2.2	53.2

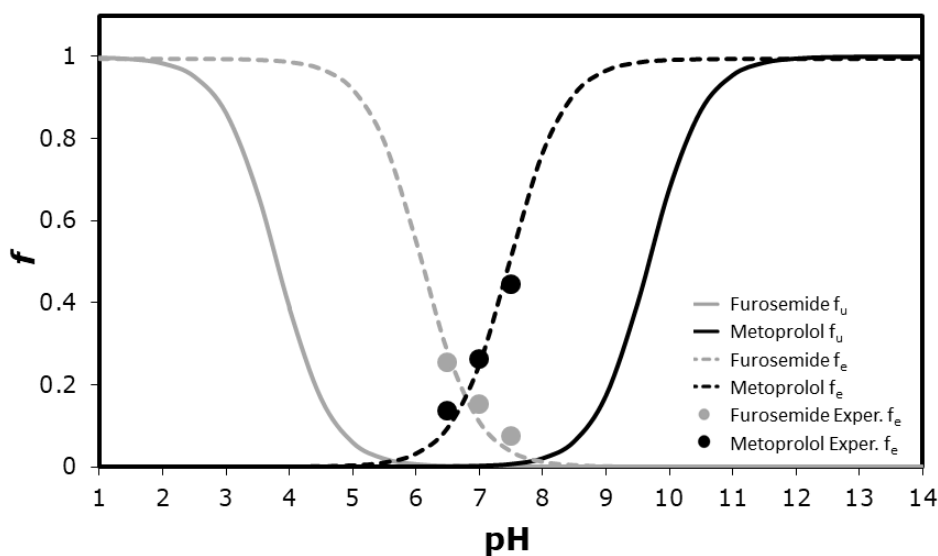


**Figure 2.** The theoretical fraction unionized ( $f_u$ ) and fraction extracted into octanol ( $f_e$ ) plots as a function of pH for furosemide and metoprolol, as well as experimental buffer-octanol partitioning of the drugs in the three pH values 6.5, 7.0, and 7.5 ( $n = 5$ ).

The effective permeability coefficient ( $P_{eff}$ , cm/sec) values of furosemide and metoprolol determined using the single-pass intestinal perfusion (SPIP) rat model, in three intestinal segments, namely proximal jejunum (pH 6.5), mid small intestine (pH 7.0), and distal ileum (pH 7.5), are presented in Figure 3. It can be seen that significant regional-dependent permeability of furosemide throughout the small intestine was evident: the permeability of furosemide gradually decreases, while the permeability of metoprolol gradually increases, as the SI segments become more distal.

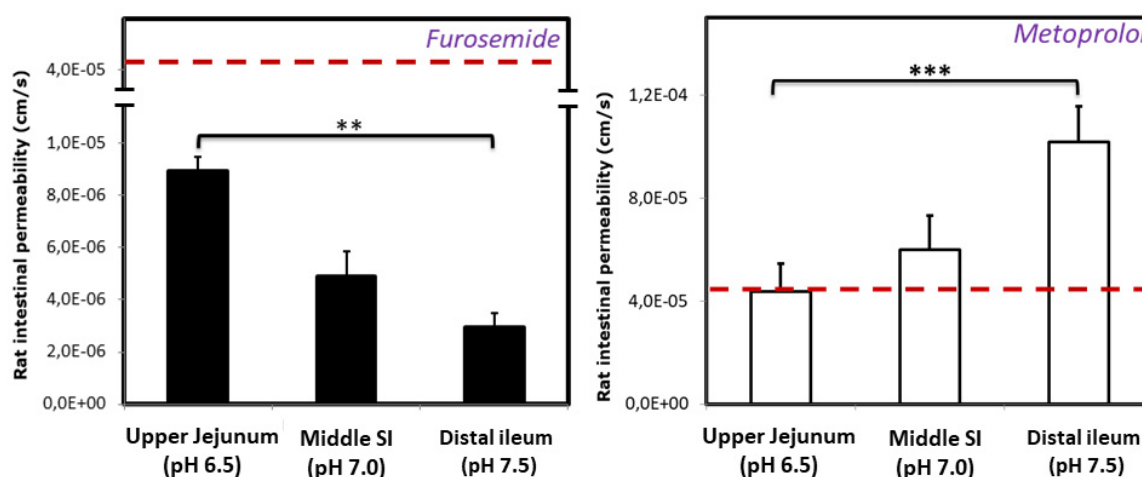


**Figure 3.** Effective permeability values ( $P_{eff}$ ; cm/s) obtained for furosemide and metoprolol after in-situ single pass perfusion to the rat proximal jejunum at pH 6.5, mid-small intestine at pH 7.0, and to the distal ileum at pH 7.5. Mean  $\pm$  S.D.;  $n = 4$  in each experimental group; \*\*  $p < 0.01$ , \*\*\*  $p < 0.001$ .

The input data regarding drug physicochemical and pharmacokinetic properties, used for in-silico simulations, are presented in Table 3. The simulated furosemide plasma concentration profile following p.o. administration is depicted in Figure 4, along with the mean profiles observed in the in-vivo studies. In addition, the observed and model predicted pharmacokinetic parameters are compared in Table 4. The presented data demonstrate that the generated model adequately describes furosemide absorption and disposition. The course of the predicted plasma profile fairly resembles the observed

data. However, certain variations are observed between the mean in-vivo data from different studies referring to the same drug dose (Figure 4, Table 4). Indeed, it has been reported that furosemide oral absorption is highly variable between individuals, e.g.,  $C_{max}$  varied three-fold, and  $t_{max}$  varied five-fold [36,37,41]; moreover, individual AUC values for 40 mg furosemide oral dose varied between 1.57 and 3.76  $\mu\text{g}\cdot\text{h}/\text{mL}$  (more than two-fold) [36,37,41], and even larger AUC values were observed in another study with the same drug dose (2.23–6.10  $\mu\text{g}\cdot\text{h}/\text{mL}$ ) [42], indicating that, regardless of the high PE(%) values in Table 4, the model predicted value of 3.66  $\mu\text{g}\cdot\text{h}/\text{mL}$  is not an overestimate of the extent of drug absorption. In addition, extensive intrasubject variability was observed for orally dosed furosemide, and these variations were attributed to the absorption process (i.e., day to day variations in physiological factors) since the repeated i.v. doses showed only marginal intrasubject variability [36,37,41]. Considering pronounced inter- and intraindividual variability in furosemide oral absorption, the simulated profile can be seen as a reasonable estimate (Figure 4). Moreover, the predicted fraction of oral drug absorption (cc. 52%) is in accordance with the values reported in the literature [36,37].

**Table 3.** The selected input parameters for furosemide absorption GastroPlus<sup>®</sup> simulation.

Parameter	Value	Source
Molecular weight (g/mol)	330.75	/
Log D (pH 7.5)	−1.0818	
Solubility at 37 °C ( $\mu\text{g}/\text{mL}$ )	19.4 (pH 1.0) 65.5 (pH 4.0) 8340.1 (pH 7.5)	experimental values
pK <sub>a</sub> (acid)	3.8	[24]
Human effective permeability, $P_{eff}$ (cm/s)	$0.4043 \times 10^{-4}$ (duodenum, jejunum) $0.2246 \times 10^{-4}$ (ileum 1 and 2) $0.1392 \times 10^{-4}$ (ileum 3, caecum, colon)	values converted using GastroPlus <sup>™</sup> integrated “permeability converter” based on experimental rat perfusion data
Diffusion coefficient ( $\text{cm}^2/\text{s}$ )	$0.7289 \times 10^{-5}$	GastroPlus <sup>™</sup> calculated value (based on molecular weight)
Mean precipitation time (s)	900	
Particle density (g/mL)	1.2	
Particle radius ( $\mu\text{m}$ )	25	GastroPlus <sup>™</sup> default values
Blood/plasma concentration ratio	1	
Plasma fraction unbound (%)	1	[24]
Clearance, CL (L/h/kg)	0.121	
Volume of distribution, Vd (L/kg)	0.043	
Distribution constant $k_{12}$ (1/h)	0.964	
Distribution constant $k_{21}$ (1/h)	1.614	
Distribution constant $k_{13}$ (1/h)	0.925	
Distribution constant $k_{32}$ (1/h)	0.708	calculated using GastroPlus <sup>™</sup> PKPlus module, based on the i.v. data [35]
Regional pH in the GIT	1.3; 6.0; 6.2; 6.4; 6.6; 6.9; 7.4; 6.4; 6.8	
Regional volume of fluid in the GIT (mL)	46.56; 40.54; 150.00; 119.30; 91.71; 68.88; 48.57; 46.44; 49.21	GastroPlus <sup>™</sup> default values for stomach, duodenum, jejunum 1, jejunum 2, ileum 1, ileum 2, ileum 3, caecum, and ascendant colon
Regional transit time in the GIT (h)	0.25; 0.26; 0.93; 0.74; 0.58; 0.42; 0.29; 4.13; 12.38	



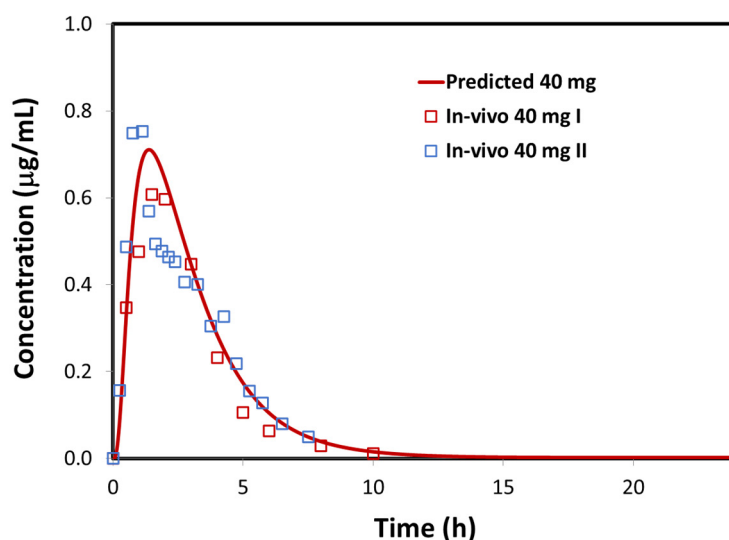


**Figure 4.** GastroPlus® simulated (line) versus mean observed (markers) plasma concentration profiles following p.o. administration of furosemide. Mean observed values represent 40 mg immediate-release (IR) tablet profile I [43] and 40 mg IR tablet profile II [37].

**Table 4.** Comparison between GastroPlus® simulated and in-vivo observed furosemide pharmacokinetic parameters following p.o. drug administration.

40 mg p.o. Dose					
Parameter	In-Vivo I <sup>a</sup>	In-Vivo II <sup>b</sup>	Predicted	PE(%) I	PE(%) II
$C_{max}$ (µg/mL)	0.61	0.75	0.71	−17.14	5.54
$t_{max}$ (h)	1.5	1.12	1.36	9.33	−22.22
$AUC_{0 \rightarrow \infty}$ (µg·h/mL)	2.13	2.44	3.66	−71.25	−50.06
$AUC_{0 \rightarrow 24 h}$ (µg·h/mL)	2.11	2.33	2.52	−19.25	−8.15
F (%)	NA	NA	52.2	NA	NA

<sup>a</sup> Refers to the mean plasma profile from [43] (40 mg IR tablet); <sup>b</sup> refers to the mean plasma profile from [37] (40 mg IR tablet); NA, not available/not applicable.

The predicted furosemide dissolution and absorption profiles following an IR oral formulation (IR tablet) are illustrated in Figure 5. The generated profiles clearly indicate that drug permeability is the limiting factor for absorption under fasted state GIT conditions. Namely, although furosemide is a low-solubility drug, due to ionization at the elevated pH conditions in the proximal SI, drug dissolution from an IR formulation is expected to be fast (>85% in 30 min). Therefore, furosemide absorption from an IR formulation is mainly governed by poor permeability. The predicted regional-dependent absorption distribution (Figure 6) further highlights the role of furosemide segmental absorption on the overall drug bioavailability. As implied by the regional-dependent permeability data, but also considering the surface area available for absorption, furosemide absorption predominantly happens in the proximal parts of the SI (76.6% of the total amount absorbed into the enterocytes), and only a minor fraction of drug (23.2% of the total amount absorbed into the enterocytes) passes into systemic circulation through mid and distal GIT regions.

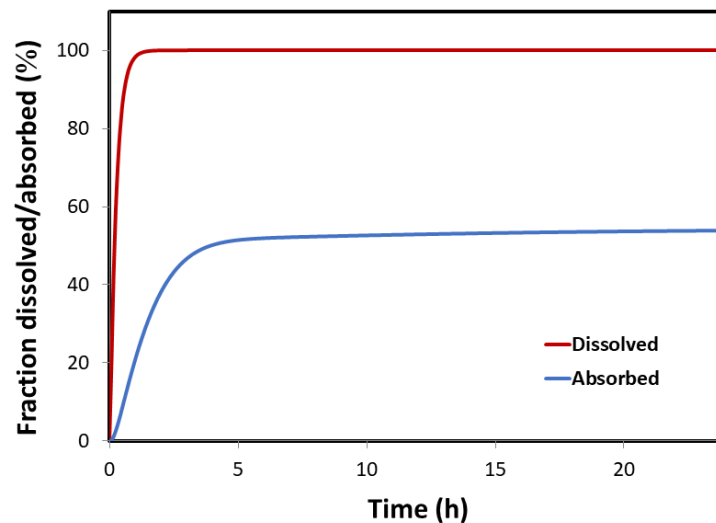


**Figure 5.** GastroPlus® simulated dissolution and absorption profiles following p.o. administration of 40 mg furosemide dose (dissolution profile was simulated using the software default Johnson equation).

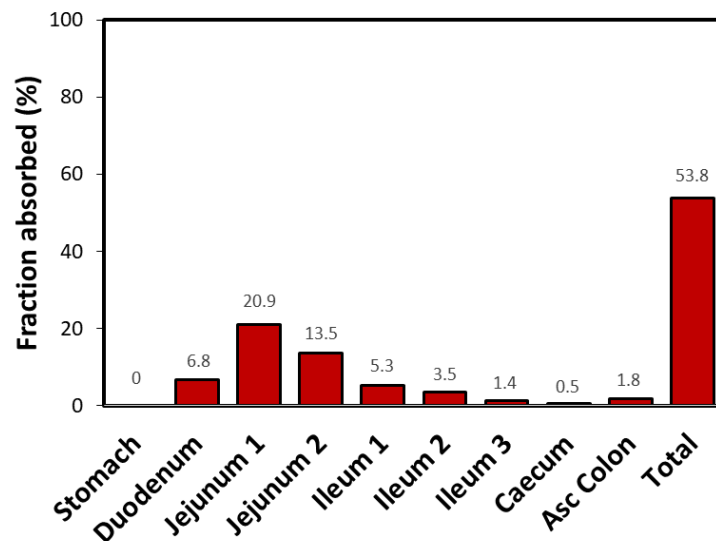


**Figure 6.** GastroPlus® simulated regional absorption of furosemide following p.o. administration of 40 mg drug dose (the simulated values refer to the fraction of drug dose that entered into the enterocytes).

The prediction results corresponding to various dissolution scenarios are presented in Figure 7b–d and Table 5. According to the simulated data, furosemide release rate from an oral formulation highly impacts the concomitant absorption process, whereas prolonged drug release rate leads to marked delay in the rate and extent of drug absorption. The estimated pharmacokinetic parameters (Table 5) indicate that furosemide bioavailability would show more than a 10-fold decrease in case the complete drug dissolution is achieved within 24 h in comparison to 15 min. A similar trend is observed for  $C_{max}$  and AUC values (17.75- and 17.38-fold decrease, respectively), while  $t_{max}$  would be prolonged (about two-fold). It is interesting to note that  $t_{max}$  increases with decrease in drug dissolution up to some point, but further decrease in drug dissolution (e.g., 85% in more than 6 h) would not cause additional delay in peak plasma concentration. This is because, after cc. 2 h, the drug leaves proximal parts of the intestine, where majority of furosemide absorption takes place, and, later on, in mid and especially distal intestine, only a small fraction of drug can be absorbed, as illustrated in Figure 7d.

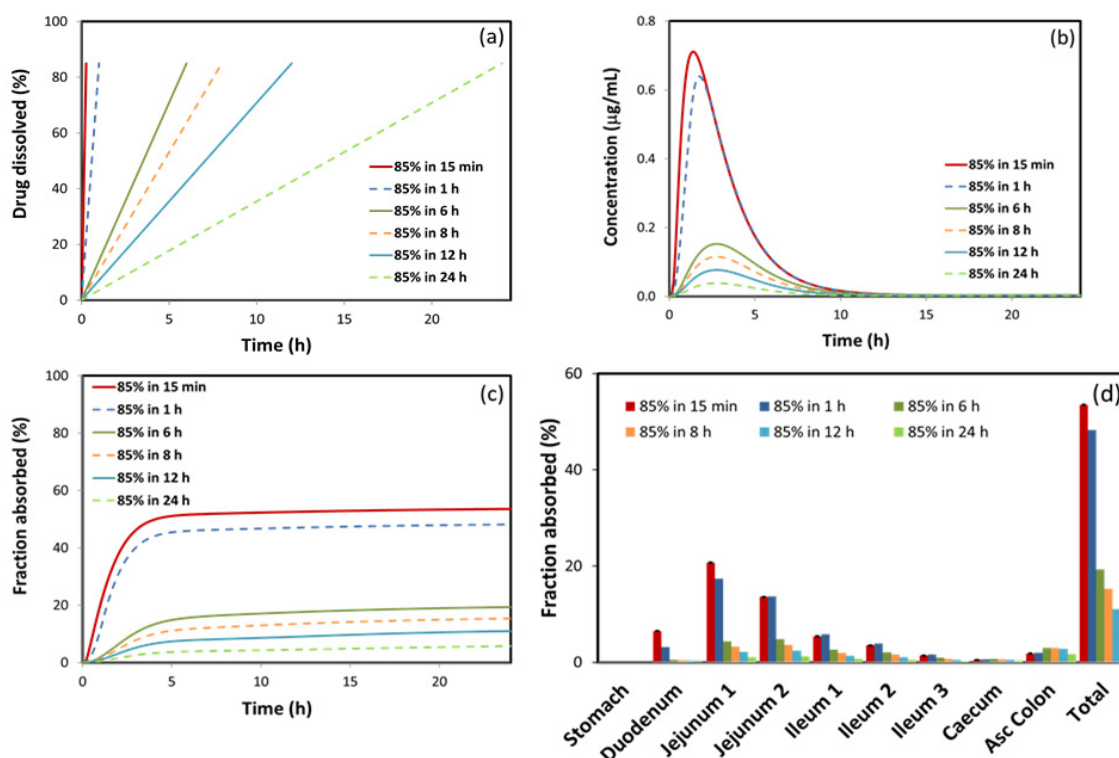


**Figure 7.** GastroPlus® simulated furosemide dissolution profiles (a); and (b) the corresponding simulated plasma profiles; (c) absorption profiles; and (d) regional absorption distribution.

**Table 5.** GastroPlus® predicted pharmacokinetic parameters for different furosemide virtual dissolution profiles from 40 mg p.o. dosage forms.

Dissolution	$C_{max}$ (µg/mL)	$t_{max}$ (h)	$AUC_{0 \rightarrow \infty}$ (µg·h/mL)	F (%)
85% in 15 min	0.71	1.36	3.65	51.91
85% in 1 h	0.64	1.76	3.71	46.35
85% in 6 h	0.15	2.80	0.80	16.64
85% in 8 h	0.11	2.80	0.61	12.73
85% in 12 h	0.08	2.80	0.41	8.65
85% in 24 h	0.04	2.80	0.21	4.36

#### 4. Discussion

BCS class IV drugs (e.g., sulfamethoxazole, ritonavir, paclitaxel, and furosemide) exhibit numerous unfavorable characteristics (low solubility and permeability, high presystemic metabolism, efflux transport), which make their oral drug delivery challenging. In addition to this, class IV drugs often demonstrate inter/intra-subject variability. Indeed, following oral administration, the absorption and bioavailability of furosemide are highly variable (37–51%) [35,41]. It has been suggested that this variability is highly dependent on the absorption process [41], which in turn is dependent on drug aqueous solubility and intestinal permeability following oral administration [1,44]. It has also been hypothesized that variable gastric/intestinal first-pass metabolism can be a factor in causing incomplete and irregular furosemide absorption in humans [45]. Despite the unfavorable class IV drug characteristics, furosemide was shown to be exceptionally useful and successful marketed drug product for the treatment of edema [17]. For this reason, we decided to investigate furosemide's solubility and in-vivo regional-dependent permeability throughout the GIT, as main parameters that guide absorption of oral drugs.

It was shown that a correlation between human  $P_{\text{eff}}$  in the jejunum and physicochemical parameters advocates that there is a high pH-dependent influence on the passive intestinal permeability in-vivo [46]. Indeed, furosemide in-vivo permeability data demonstrate a downward trend towards the distal intestinal segments as the pH gradually increases, a trend that can be expected for acidic drugs, since the pH in the intestinal lumen gradually increases towards distal SI regions (Figure 3). Many BCS class IV drugs are substrates for efflux transporters [47]. There is some evidence that furosemide might be a substrate for efflux transporters [48,49]; thus, such permeability trend could also be influenced by the P-glycoprotein (P-gp) transporter in which expression levels are increased from proximal to distal SI segments [6,50–52]. Since metoprolol's intestinal permeability is passive and does not involve carrier-mediated absorption, it exhibited pH-dependent intestinal permeability, with reverse tendency compared to furosemide; as a basic drug, metoprolol showed upward increase in permeability towards distal SI segments with rising pH values (Figure 3). At any point throughout the SI, furosemide exhibited significantly lower permeability than the benchmark (metoprolol's jejunum permeability), which confirms its BCS low-permeability classification and incomplete absorption. Despite the fact that furosemide is a low-permeability drug, the higher permeability in the proximal intestinal regions provides a window for furosemide absorption, and we posit that this is one of the main reasons for furosemide's sufficient bioavailability and success as a marketed drug. Theoretical  $f_u$  and  $f_e$  as a function of pH were found to be in excellent correlation to these in-vivo data. In addition, in-silico modeling indicated that furosemide dissolution from an IR formulation would be fairly complete before the drug leaves proximal SI (Figure 5), although the drug is generally classified as low-soluble, enabling timely delivery of the dissolved drug to the distinct absorption site. Complete furosemide dissolution under physiological conditions is also confirmed by the experimental solubility results (Table 1).

Furosemide Log D studies showed higher partition coefficient in comparison to metoprolol at pH 6.5, whereas, in the in-vivo intestinal perfusion experiment, furosemide showed significantly lower jejunum permeability than metoprolol (Figure 1). A possible reason for this difference in the partitioning and in-vivo permeability can be the polar surface area (PSA) of both drugs [53]. A sigmoidal relationship between the fraction absorbed following oral administration and the dynamic polar surface area was reported in the past [54–56]. It was shown that orally administered drugs with large PSA (>120) are hardly absorbed by the passive transcellular route, while drugs with a small PSA (<60) are almost completely absorbed [55,56]. This is in agreement with our results, as furosemide has much higher PSA (127.7) than metoprolol (53.2) [54,55]. Another reason for the difference in the partitioning and in-vivo permeability may be the presence of active efflux transport involved in the intestinal permeability. The influence of efflux transport at pH 6.5 (proximal intestinal segments) could decrease furosemide's permeability in-vivo, which was not accounted for in the octanol partitioning studies.

The Log P value of furosemide (2.3) is in the close proximity to that of metoprolol (2.2), pointing to high permeability (Table 2). However, the Log P calculation is based on the unionized drug fraction, and, since furosemide has acidic nature it is likely that, once it passes the acidic stomach environment, it will mostly be in ionized form (the pH throughout the GIT varies from 5.9–6.3 in the proximal SI to 7.4–7.8 in distal SI segments; pH in the colon is fluctuating between pH 5–8 [57]); therefore the high furosemide Log P is not in correspondence with permeability in-vivo. Thus, we posit that no single parameter can be used for measuring the drug absorption process, but rather, a combination of physicochemical parameters and in-vitro and in-vivo findings, as well as careful consideration of inclusion criteria prior to making decisions. Despite the high Log P value for furosemide, it was indeed confirmed that furosemide is a BCS class IV drug, based on both the solubility data (Table 1) and the intestinal permeability (Figure 3).

Suitable formulation is the main approach to create an efficacious drug product for the administration of BCS class IV drugs [47]. Absorption windows in the proximal intestinal segments can restrict the oral drug bioavailability and can be a significant limitation for the development of CR drug formulation. The underlying reasons are mechanistically explained by our in-silico results (Figure 7). As mentioned, furosemide permeability results revealed acceptable permeability in the

proximal segments of the SI, which is presumably the reason why furosemide has appropriate drug bioavailability, despite being a BCS class IV drug. However, since CR products release the drug over 12–24 h, mostly in the colon, (transit time throughout the small intestine is 3–4 h [58]), the fact that furosemide is mainly absorbed from proximal SI segments, (with decreased permeability at distant GIT segments) prevents the formulation of furosemide as a CR product, as shown previously [21,59,60]. However, we believe that formulations based on gastro-retentive dosage forms (GRDF) can be shown as prosperous for furosemide [61]. There are several similar examples in the literature where absorption window occurs in the upper GI, and this has been used to create GDRF formulations to improve the drug absorption, such as riboflavin [62] and levodopa [59,63].

Several types of bariatric surgeries (specifically Roux-en-Y gastric bypass and mini bypass) result in bypassing the upper SI. In cases where the absorption window is indeed in this upper SI region, the absorption following the bariatric surgery can be hampered vastly, since the actual segment responsible for the majority of absorption is bypassed [64–66].

## 5. Conclusions

Regional-dependent permeability throughout the small intestine was evident for furosemide. The permeability of furosemide gradually decreases throughout the small intestine as a function of the pH change in the intestinal lumen. However, at any point throughout the small intestine, furosemide exhibited significantly lower permeability than the benchmark of metoprolol's permeability in the jejunum, which may explain the incomplete absorption of the drug. We propose that, for a drug to be classified as BCS low-permeability, its intestinal permeability should not match/exceed the low/high class benchmark anywhere throughout the intestinal tract, as well as is not restricted necessarily to the jejunum. Nevertheless, low-permeable drugs should not be treated as 'unfavorable' by default; instead, therapeutic potential and suitable formulation strategies should be considered on a case-by-case basis, taking into account the overall results of in-vitro, in-vivo, and in-silico testing, throughout the entire gastrointestinal tract.

**Author Contributions:** M.M., M.Z., I.R., S.C. and A.D. worked on conceptualization, methodology, investigation, analyzed the data, and outlined the manuscript. S.C. worked on software investigation. Writing: S.C., A.D. and M.M. prepared the original draft of the article, and M.Z. and I.R. contributed to the writing-review and editing of the full version. All authors have read and agreed to the published version of the manuscript.

**Funding:** This work received no external funding.

**Conflicts of Interest:** The authors declare no conflict of interest.

## References

1. Amidon, G.L.; Lennernäs, H.; Shah, V.P.; Crison, J.R. A theoretical basis for a biopharmaceutical drug classification: The correlation of in vitro drug product dissolution and in vivo bioavailability. *Pharm. Res.* **1995**, *12*, 413–420. [[CrossRef](#)]
2. Dahan, A.; Miller, J.M.; Amidon, G.L. Prediction of solubility and permeability class membership: Provisional BCS classification of the world's top oral drugs. *AAPS J.* **2009**, *11*, 740–746. [[CrossRef](#)]
3. Dahan, A.; Beig, A.; Lindley, D.; Miller, J.M. The solubility-permeability interplay and oral drug formulation design: Two heads are better than one. *Adv. Drug Deliv. Rev.* **2016**, *101*, 99–107. [[CrossRef](#)]
4. Dahan, A.; Miller, J.M. The solubility-permeability interplay and its implications in formulation design and development for poorly soluble drugs. *AAPS J.* **2012**, *14*, 244–251. [[CrossRef](#)]
5. Miller, J.M.; Beig, A.; Carr, R.A.; Webster, G.K.; Dahan, A. The solubility-permeability interplay when using cosolvents for solubilization: Revising the way we use solubility-enabling formulations. *Mol. Pharm.* **2012**, *9*, 581–590. [[CrossRef](#)]
6. Dahan, A.; Amidon, G.L. Segmental dependent transport of low permeability compounds along the small intestine due to P-Glycoprotein: The role of efflux transport in the oral absorption of BCS class III drugs. *Mol. Pharm.* **2009**, *6*, 19–28. [[CrossRef](#)]

7. Dahan, A.; West, B.T.; Amidon, G.L. Segmental-dependent membrane permeability along the intestine following oral drug administration: Evaluation of a triple single-pass intestinal perfusion (TSPiP) approach in the rat. *Eur. J. Pharm. Sci.* **2009**, *36*, 320–329. [[CrossRef](#)]
8. Fairstein, M.; Swissa, R.; Dahan, A. Regional-dependent intestinal permeability and BCS classification: Elucidation of pH-related complexity in rats using pseudoephedrine. *AAPS J.* **2013**, *15*, 589–597. [[CrossRef](#)]
9. Lozoya-Agullo, I.; Zur, M.; Beig, A.; Fine, N.; Cohen, Y.; Gonzalez-Alvarez, M.; Merino-Sanjuan, M.; Gonzalez-Alvarez, I.; Bermejo, M.; Dahan, A. Segmental-dependent permeability throughout the small intestine following oral drug administration: Single-pass vs. Doluisio approach to in-situ rat perfusion. *Int. J. Pharm.* **2016**, *515*, 201–208. [[CrossRef](#)]
10. Markovic, M.; Zur, M.; Dahan, A.; Cvijić, S. Biopharmaceutical characterization of rebamipide: The role of mucus binding in regional-dependent intestinal permeability. *Eur. J. Pharm. Sci.* **2020**, *152*, 105440. [[CrossRef](#)]
11. Zur, M.; Hanson, A.S.; Dahan, A. The complexity of intestinal permeability: Assigning the correct BCS classification through careful data interpretation. *Eur. J. Pharm. Sci.* **2014**, *61*, 11–17. [[CrossRef](#)]
12. U.S. Department of Health and Human Services, Food and Drug Administration; Center for Drug Evaluation and Research (CDER). *Waiver of In-Vivo Bioavailability and Bioequivalence Studies for Immediate-Release Solid Oral Dosage Forms Based on a Biopharmaceutics Classification System; Guidance for Industry*; Center for Drug Evaluation and Research (CDER): Silver Spring, MD, USA, 2017.
13. Dahan, A.; Wolk, O.; Kim, Y.H.; Ramachandran, C.; Crippen, G.M.; Takagi, T.; Bermejo, M.; Amidon, G.L. Purely in silico BCS classification: Science based quality standards for the world's drugs. *Mol. Pharm.* **2013**, *10*, 4378–4390. [[CrossRef](#)]
14. Takagi, T.; Ramachandran, C.; Bermejo, M.; Yamashita, S.; Yu, L.X.; Amidon, G.L. A provisional biopharmaceutical classification of the top 200 oral drug products in the United States, Great Britain, Spain, and Japan. *Mol. Pharm.* **2006**, *3*, 631–643. [[CrossRef](#)]
15. Wolk, O.; Agbaria, R.; Dahan, A. Provisional in-silico biopharmaceutics classification (BCS) to guide oral drug product development. *Drug Des. Dev. Ther.* **2014**, *8*, 1563–1575. [[CrossRef](#)]
16. Lindenberg, M.; Kopp, S.; Dressman, J.B. Classification of orally administered drugs on the World Health Organization model list of essential medicines according to the biopharmaceutics classification system. *Eur. J. Pharm. Biopharm.* **2004**, *58*, 265–278. [[CrossRef](#)]
17. Furosemide Tablets, United States Pharmacopeia Label. Available online: [https://www.accessdata.fda.gov/drugsatfda\\_docs/label/2016/018487s043lbl.pdf](https://www.accessdata.fda.gov/drugsatfda_docs/label/2016/018487s043lbl.pdf) (accessed on 11 July 2020).
18. Ellison, D.H.; Felker, G.M. Diuretic Treatment in Heart Failure. *N. Engl. J. Med.* **2017**, *377*, 1964–1975. [[CrossRef](#)]
19. Hammarlund-Udenaes, M.; Benet, L.Z. Furosemide pharmacokinetics and pharmacodynamics in health and disease—An update. *J. Pharmacokinet. Biopharm.* **1989**, *17*, 1–46. [[CrossRef](#)]
20. Dahan, A.; Wolk, O.; Zur, M.; Amidon, G.L.; Abrahamsson, B.; Cristofolletti, R.; Groot, D.W.; Kopp, S.; Langguth, P.; Polli, J.E.; et al. Biowaiver monographs for immediate-release solid oral dosage forms: Codeine phosphate. *J. Pharm. Sci.* **2014**, *103*, 1592–1600. [[CrossRef](#)]
21. Markovic, M.; Zur, M.; Fine-Shamir, N.; Haimov, E.; González-Álvarez, I.; Dahan, A. Segmental-dependent solubility and permeability as key factors guiding controlled release drug product development. *Pharmaceutics* **2020**, *12*, 295. [[CrossRef](#)]
22. Zur, M.; Cohen, N.; Agbaria, R.; Dahan, A. The biopharmaceutics of successful controlled release drug product: Segmental-dependent permeability of glipizide vs. metoprolol throughout the intestinal tract. *Int. J. Pharm.* **2015**, *489*, 304–310. [[CrossRef](#)]
23. Zur, M.; Gasparini, M.; Wolk, O.; Amidon, G.L.; Dahan, A. The low/high BCS permeability class boundary: Physicochemical comparison of metoprolol and labetalol. *Mol. Pharm.* **2014**, *11*, 1707–1714. [[CrossRef](#)]
24. Granero, G.E.; Longhi, M.R.; Mora, M.J.; Junginger, H.E.; Midha, K.K.; Shah, V.P.; Stavchansky, S.; Dressman, J.B.; Barends, D.M. Biowaiver monographs for immediate release solid oral dosage forms: Furosemide. *J. Pharm. Sci.* **2010**, *99*, 2544–2556. [[CrossRef](#)] [[PubMed](#)]
25. Wagner, J.G.; Sedman, A.J. Quantitation of rate of gastrointestinal and buccal absorption of acidic and basic drugs based on extraction theory. *J. Pharmacokinet. Biopharm.* **1973**, *1*, 23–50. [[CrossRef](#)]
26. Winne, D. Shift of pH-absorption curves. *J. Pharmacokinet. Biopharm.* **1977**, *5*, 53–94. [[CrossRef](#)]
27. Berthod, A.; Carda-Broch, S.; Garcia-Alvarez-Coque, M.C. Hydrophobicity of ionizable compounds. A theoretical study and measurements of diuretic octanol–water partition coefficients by countercurrent chromatography. *Anal. Chem.* **1999**, *71*, 879–888. [[CrossRef](#)]

28. Henchoz, Y.; Guillaume, D.; Martel, S.; Rudaz, S.; Veuthey, J.L.; Carrupt, P.A. Fast log P determination by ultra-high-pressure liquid chromatography coupled with UV and mass spectrometry detections. *Anal. Bioanal. Chem.* **2009**, *394*, 1919–1930. [[CrossRef](#)]
29. Teksin, Z.S.; Hom, K.; Balakrishnan, A.; Polli, J.E. Ion pair-mediated transport of metoprolol across a three lipid-component PAMPA system. *J. Control. Release Off. J. Control. Release Soc.* **2006**, *116*, 50–57. [[CrossRef](#)]
30. Lozoya-Agullo, I.; Gonzalez-Alvarez, I.; Zur, M.; Fine-Shamir, N.; Cohen, Y.; Markovic, M.; Garrigues, T.M.; Dahan, A.; Gonzalez-Alvarez, M.; Merino-Sanjuán, M.; et al. Closed-loop doluisio (colon, small intestine) and single-pass intestinal perfusion (colon, jejunum) in rat—Biophysical model and predictions based on Caco-2. *Pharm. Res.* **2017**, *35*, 2. [[CrossRef](#)]
31. Lozoya-Agullo, I.; Zur, M.; Fine-Shamir, N.; Markovic, M.; Cohen, Y.; Porat, D.; Gonzalez-Alvarez, I.; Gonzalez-Alvarez, M.; Merino-Sanjuan, M.; Bermejo, M.; et al. Investigating drug absorption from the colon: Single-pass vs. Doluisio approaches to in-situ rat large-intestinal perfusion. *Int. J. Pharm.* **2017**, *527*, 135–141. [[CrossRef](#)]
32. Lozoya-Agullo, I.; Zur, M.; Wolk, O.; Beig, A.; Gonzalez-Alvarez, I.; Gonzalez-Alvarez, M.; Merino-Sanjuan, M.; Bermejo, M.; Dahan, A. In-situ intestinal rat perfusions for human Fabs prediction and BCS permeability class determination: Investigation of the single-pass vs. the Doluisio experimental approaches. *Int. J. Pharm.* **2015**, *480*, 1–7. [[CrossRef](#)]
33. Dahan, A.; Miller, J.M.; Hilfinger, J.M.; Yamashita, S.; Yu, L.X.; Lennernas, H.; Amidon, G.L. High-permeability criterion for BCS classification: Segmental/pH dependent permeability considerations. *Mol. Pharm.* **2010**, *7*, 1827–1834. [[CrossRef](#)]
34. Wolk, O.; Markovic, M.; Porat, D.; Fine-Shamir, N.; Zur, M.; Beig, A.; Dahan, A. Segmental-dependent intestinal drug permeability: Development and model validation of in silico predictions guided by in vivo permeability values. *J. Pharm. Sci.* **2019**, *108*, 316–325. [[CrossRef](#)]
35. Kelly, M.R.; Cutler, R.E.; Forrey, A.W.; Kimpel, B.M. Pharmacokinetics of orally administered furosemide. *Clin. Pharmacol. Ther.* **1974**, *15*, 178–186. [[CrossRef](#)]
36. Benet, L.Z. Pharmacokinetics/pharmacodynamics of furosemide in man: A review. *J. Pharmacokinet. Biopharm.* **1979**, *7*, 1–27. [[CrossRef](#)]
37. Hammarlund, M.M.; Paalzow, L.K.; Odland, B. Pharmacokinetics of furosemide in man after intravenous and oral administration. Application of moment analysis. *Eur. J. Clin. Pharmacol.* **1984**, *26*, 197–207. [[CrossRef](#)]
38. Agoram, B.; Woltosz, W.S.; Bolger, M.B. Predicting the impact of physiological and biochemical processes on oral drug bioavailability. *Adv. Drug Deliv. Rev.* **2001**, *50*, S41–S67. [[CrossRef](#)]
39. Lin, L.; Wong, H. Predicting oral drug absorption: Mini review on physiologically-based pharmacokinetic models. *Pharmaceutics* **2017**, *9*, 41. [[CrossRef](#)]
40. Lu, A.T.K.; Frisella, M.E.; Johnson, K.C. Dissolution modeling: Factors affecting the dissolution rates of polydisperse powders. *Pharm. Res.* **1993**, *10*, 1308–1314. [[CrossRef](#)]
41. Grahnen, A.; Hammarlund, M.; Lundqvist, T. Implications of intraindividual variability in bioavailability studies of furosemide. *Eur. J. Clin. Pharmacol.* **1984**, *27*, 595–602. [[CrossRef](#)]
42. Waller, E.S.; Hamilton, S.F.; Massarella, J.W.; Sharanevych, M.A.; Smith, R.V.; Yakatan, G.J.; Doluisio, J.T. Disposition and absolute bioavailability of furosemide in healthy males. *J. Pharm. Sci.* **1982**, *71*, 1105–1108. [[CrossRef](#)]
43. Beermann, B.; Midskov, C. Reduced bioavailability and effect of furosemide given with food. *Eur. J. Clin. Pharmacol.* **1986**, *29*, 725–727. [[CrossRef](#)]
44. Dahan, A.; Lennernas, H.; Amidon, G.L. The fraction dose absorbed, in humans, and high jejunal human permeability relationship. *Mol. Pharm.* **2012**, *9*, 1847–1851. [[CrossRef](#)]
45. Lee, M.G.; Chiou, W.L. Evaluation of potential causes for the incomplete bioavailability of furosemide: Gastric first-pass metabolism. *J. Pharm. Biopharm.* **1983**, *11*, 623–640. [[CrossRef](#)]
46. Dahlgren, D.; Lennernas, H. Intestinal permeability and drug absorption: Predictive experimental, computational and in vivo approaches. *Pharmaceutics* **2019**, *11*, 411. [[CrossRef](#)]
47. Ghadi, R.; Dand, N. BCS class IV drugs: Highly notorious candidates for formulation development. *J. Control. Release Off. J. Control. Release Soc.* **2017**, *248*, 71–95. [[CrossRef](#)]
48. Flanagan, S.D.; Cummins, C.L.; Susanto, M.; Liu, X.; Takahashi, L.H.; Benet, L.Z. Comparison of furosemide and vinblastine secretion from cell lines overexpressing multidrug resistance protein (P-glycoprotein) and multidrug resistance-associated proteins (MRP1 and MRP2). *Pharmacology* **2002**, *64*, 126–134. [[CrossRef](#)]

49. Takahashi, M.; Washio, T.; Suzuki, N.; Igeta, K.; Fujii, Y.; Hayashi, M.; Shirasaka, Y.; Yamashita, S. Characterization of gastrointestinal drug absorption in cynomolgus monkeys. *Mol. Pharm.* **2008**, *5*, 340–348. [[CrossRef](#)]
50. Cao, X.; Yu, L.X.; Barbaciru, C.; Landowski, C.P.; Shin, H.C.; Gibbs, S.; Miller, H.A.; Amidon, G.L.; Sun, D. Permeability dominates in vivo intestinal absorption of P-gp substrate with high solubility and high permeability. *Mol. Pharm.* **2005**, *2*, 329–340. [[CrossRef](#)]
51. Englund, G.; Rorsman, F.; Rönnblom, A.; Karlbom, U.; Lazorova, L.; Gråsjö, J.; Kindmark, A.; Artursson, P. Regional levels of drug transporters along the human intestinal tract: Co-expression of ABC and SLC transporters and comparison with Caco-2 cells. *Eur. J. Pharm. Sci.* **2006**, *29*, 269–277. [[CrossRef](#)]
52. Zimmermann, C.; Gutmann, H.; Hruz, P.; Gutzwiller, J.-P.; Beglinger, C.; Drewe, J. Mapping of multidrug resistance gene 1 and multidrug resistance-associated protein isoform 1 to 5 mRNA expression along the human intestinal tract. *Drug Metab. Dispos.* **2005**, *33*, 219. [[CrossRef](#)]
53. Winiwarter, S.; Bonham, N.M.; Ax, F.; Hallberg, A.; Lennernäs, H.; Karlén, A. Correlation of human jejunal permeability (in vivo) of drugs with experimentally and theoretically derived parameters. A multivariate data analysis approach. *J. Med. Chem.* **1998**, *41*, 4939–4949. [[CrossRef](#)]
54. Clark, D.E. Rapid calculation of polar molecular surface area and its application to the prediction of transport phenomena. 1. Prediction of intestinal absorption. *J. Pharm. Sci.* **1999**, *88*, 807–814. [[CrossRef](#)]
55. Palm, K.; Luthman, K.; Ungell, A.-L.; Strandlund, G.; Beigi, F.; Lundahl, P.; Artursson, P. Evaluation of dynamic polar molecular surface area as predictor of drug absorption: Comparison with other computational and experimental predictors. *J. Med. Chem.* **1998**, *41*, 5382–5392. [[CrossRef](#)]
56. Ertl, P.; Rohde, B.; Selzer, P. Fast calculation of molecular polar surface area as a sum of fragment-based contributions and its application to the prediction of drug transport properties. *J. Med. Chem.* **2000**, *43*, 3714–3717. [[CrossRef](#)]
57. Koziolok, M.; Grimm, M.; Becker, D.; Iordanov, V.; Zou, H.; Shimizu, J.; Wanke, C.; Garbacz, G.; Weitschies, W. Investigation of pH and temperature profiles in the GI tract of fasted human subjects using the intellicap<sup>®</sup> system. *J. Pharm. Sci.* **2015**, *104*, 2855–2863. [[CrossRef](#)]
58. Davis, S.S.; Hardy, J.G.; Fara, J.W. Transit of pharmaceutical dosage forms through the small intestine. *Gut* **1986**, *27*, 886–892. [[CrossRef](#)]
59. Streubel, A.; Siepmann, J.; Bodmeier, R. Drug delivery to the upper small intestine window using gastroretentive technologies. *Curr. Opin. Pharmacol.* **2006**, *6*, 501–508. [[CrossRef](#)]
60. Clear, N.J.; Milton, A.; Humphrey, M.; Henry, B.T.; Wulff, M.; Nichols, D.J.; Anziano, R.J.; Wilding, I. Evaluation of the Intelisite capsule to deliver theophylline and frusemide tablets to the small intestine and colon. *Eur. J. Pharm. Sci. Off. J. Eur. Fed. Pharm. Sci.* **2001**, *13*, 375–384. [[CrossRef](#)]
61. Darandale, S.S.; Vavia, P.R. Design of a gastroretentive mucoadhesive dosage form of furosemide for controlled release. *Acta Pharm. Sin. B* **2012**, *2*, 509–517. [[CrossRef](#)]
62. Kagan, L.; Lapidot, N.; Afargan, M.; Kirmayer, D.; Moor, E.; Mardor, Y.; Friedman, M.; Hoffman, A. Gastroretentive accordion pill: Enhancement of riboflavin bioavailability in humans. *J. Control. Release Off. J. Control. Release Soc.* **2006**, *113*, 208–215. [[CrossRef](#)]
63. Klausner, E.A.; Eyal, S.; Lavy, E.; Friedman, M.; Hoffman, A. Novel levodopa gastroretentive dosage form: In-vivo evaluation in dogs. *J. Control. Release* **2003**, *88*, 117–126. [[CrossRef](#)]
64. Israel, S.; Elinav, H.; Elazary, R.; Porat, D.; Gibori, R.; Dahan, A.; Azran, C.; Horwitz, E. Case report of increased exposure to antiretrovirals following sleeve gastrectomy. *Antimicrob. Agents Chemother.* **2020**, *64*. [[CrossRef](#)]
65. Porat, D.; Dahan, A. Medication management after bariatric surgery: Providing optimal patient care. *J. Clin. Med.* **2020**, *9*, 1511. [[CrossRef](#)]
66. Porat, D.; Markovic, M.; Zur, M.; Fine-Shamir, N.; Azran, C.; Shaked, G.; Czeiger, D.; Vaynshtein, J.; Replyanski, I.; Sebbag, G.; et al. Increased paracetamol bioavailability after sleeve gastrectomy: A crossover pre- vs. post-operative clinical trial. *J. Clin. Med.* **2019**, *8*, 1949. [[CrossRef](#)]

**Publisher’s Note:** MDPI stays neutral with regard to jurisdictional claims in published maps and institutional affiliations.



© 2020 by the authors. Licensee MDPI, Basel, Switzerland. This article is an open access article distributed under the terms and conditions of the Creative Commons Attribution (CC BY) license (<http://creativecommons.org/licenses/by/4.0/>).